TECHNICAL REPORT BRL-TR-3369

BRL

LASER-BASED SPECTROSCOPIC STUDIES OF PROPELLANT-LIKE LOW-PRESSURE FLAMES

STEPHEN L. HOWARD
RANDY J. LOCKE
ROSARIO C. SAUSA
ANTHONY J. KOTLAR
ANDRZEJ W. MIZIOLEK

JULY 1992

U.S. ARMY LABORATORY COMMAND

BALLISTIC RESEARCH LABORATORY
ABERDEEN PROVING GROUND, MARYLAND

NOTICES

Destroy this report when it is no longer needed. DO NOT return it to the originator.

Additional copies of this report may be obtained from the National Technical Information Service, U.S. Department of Commerce, 5285 Port Royal Road, Springfield, VA 22161.

The findings of this report are not to be construed as an official Department of the Army position, unless so designated by other authorized documents.

The use of trade names or manufacturers' names in this report does not constitute indorsement of any commercial product.

REPORT DOCUMENTATION PAGE

Form Approved
OMB No. 0704-0188

1. AGENCY USE ONLY (Leave blank)	2. REPORT DATE	3. REPORT TYPE AND DATES COVERED
	July 1992	Final Oct 1989 - Jan 1991

4. TITLE AND SUBTITLE

Laser-Based Spectroscopic Studies of Propellant-Like Low-Pressure Flames

5. FUNDING NUMBERS

PR: 1L161102AH43

6. AUTHOR(S)

Stephen L. Howard, Randy J. Locke, Rosario C. Sausa, Anthony J. Kotlar, Andrzej W. Miziolek

7. PERFORMING ORGANIZATION NAME(S) AND ADDRESS(ES)

U. S. Army Ballistic Research Laboratory
ATTN: SLCBR-IB-P
Aberdeen Provind Ground, MD 21005-5066

8. PERFORMING ORGANIZATION REPORT NUMBER

9. SPONSORING/MONITORING AGENCY NAME(S) AND ADDRESS(ES)

U. S. Army Ballistic Research Laboratory
ATTN: SLCBR-DD-T
Aberdeen Proving Ground, MD 21005-5066

10. SPONSORING/MONITORING AGENCY REPORT NUMBER

BRL-TR-3369

11. SUPPLEMENTARY NOTES

12a. DISTRIBUTION/AVAILABILITY STATEMENT

Approved for Public Release; Distribution Unlimited

12b. DISTRIBUTION CODE

13. ABSTRACT (Maximum 200 words)

A new generation of flat flame burner for characterization of one-dimensional premixed laminar flames has been developed to study the detailed flame chemistry relevant to gaseous flames of burning propellants. Experimental results provide temperature and species profiles which are necessary to validate flame models that are being developed to simulate propellant combustion. This facility is an integrated apparatus that presently consists of various laser-based diagnostic tools and thermocouples. This report discusses results obtained from $C_2H_4/O_2/Ar$ and H_2/NO_2 low-pressure flames. Profiles for O, H, OH, CH_3, HCO, NO and NO_2 in the appropriate flames were obtained. Temperature profiles were taken of the flames and compared to temperatures obtained by OH laser-induced fluorescence. NO resonance-enhanced multiphoton ionization thermometry was tried and the results discussed. Comparison of $C_2H_4/O_2/Ar$ results are compared with modelling efforts.

14. SUBJECT TERMS

Flames; Laser Induced Fluorescence; Resonance-Enhanced Ionization

15. NUMBER OF PAGES

29

16. PRICE CODE

17. SECURITY CLASSIFICATION OF REPORT	18. SECURITY CLASSIFICATION OF THIS PAGE	19. SECURITY CLASSIFICATION OF ABSTRACT	20. LIMITATION OF ABSTRACT
UNCLASSIFIED	UNCLASSIFIED	UNCLASSIFIED	UL

INTENTIONALLY LEFT BLANK

TABLE OF CONTENTS

INTENTIONALLY LEFT BLANK

LIST OF FIGURES

LIST OF TABLES

INTENTIONALLY LEFT BLANK

ACKNOWLEDGEMENTS

We would like to thank the Office of Naval Research (ONR Contract No. MIPRN0001490MP24054), the Army Research Office (Contract No. DAAL0387K0066) and the BRL combustion Research mission program for funding of this work. Support of Stephen L Howard and Randy J. Locke by the National Research Council Research Associate Program is also gratefully acknowledged. We would also like to thank Professor T. A. Cool and his students J. S. Bernstein and J. B. Choi, Cornell University, School of Applied and Engineering Physics, Ithaca, New York for cooperative assistance in obtaining CH_3 and HCO profiles, modelling and useage of their REMPI power supply filter.

Randy J. Locke is currently employed at:

Sverdrup Technology, Inc.
LeRC Group
Mailstop SVR-2
2001 Aerospace Parkway
Brook Park, OH 44142 .

INTENTIONALLY LEFT BLANK

1. INTRODUCTION

A good deal is yet unknown about the actual reaction mechanisms in propulsion flames. It is becoming increasingly important that such mechanisms are known. Propellant selection and optimization are dependent upon burning characteristics and the products formed. Spatially resolved temperature and species profiles in $C_2H_4/O_2/Ar$ and H_2/NO_2 low-pressure flames are needed to better understand the chemistry occurring in propellant flames and to validate existing chemical flame models in reference to assumed chemical flame mechanisms and rate constant data that such models require. While much modeling effort has been expended in an attempt to understand these processes, many of the reactions involved in these two flames are believed to be a subset of the more complex network of reactions needed for flame models that are being developed to simulate hydrocarbon and composite solid propellant combustion.

Over the past few decades, there has been significant progress in the study of the structure of flames. Several laser spectroscopic techniques such as laser-induced fluorescence (LIF) and multiphoton techniques such as resonance-enhanced multiphoton ionization (REMPI) have yielded species concentration measurements with a good degree of selectivity and spatial resolution (Lucht et al. 1983, Alden et al. 1982, Goldsmith 1983, Eckbreth 1988). These techniques are very attractive because they are complementary, usually nonintrusive, and offer good sensitivity with detection limits within sub-ppm levels. Since laser energy can easily be focussed, spatial resolution of less than 100 microns is easily achieved. However, these techniques do require specific knowledge of the absorption spectrum of the species of interest. Also required is knowledge of the emission spectrum for LIF and the electronic states and ionization potentials for REMPI of each species of interest. While high resolution spectral overlap with interfering species is usually infrequent for these simple flames, the above information is also required for any possible interfering species.

Flame temperatures have also been measured by LIF of the OH radical employing its well-known $A\ ^2\Sigma^+ \leftarrow X\ ^2\Pi_i$ (1,0) band near 281 nm. The OH radical has been the subject of many studies since it is ubiquitous in most flame systems and can be modeled spectroscopically. For these measurements, accurate transition probabilities and quenching rates due to the presence of other species are also required

(Cattolica and Mataga 1991) as well as assuming a local thermal equilibrium is established so that a Boltzmann energy distribution analysis can be applied.

This report covers temperature profile measurements obtained by inert coated (Kent 1970) Pt/Pt-Rh(10%) thermocouples in $C_2H_4/O_2/Ar$ and H_2/NO_2 low-pressure flames. Also included are species profiles of O, H, OH, CH_3, HCO, NO and NO_2 in the respective flames. Comparison of experimental species profiles for the $C_2H_4/O_2/Ar$ flame with those generated by computer modelling is also discussed. Model results required the temperature profile as measured by thermocouple as input so that solutions of the energy equations would converge.

2. EXPERIMENTAL

The flames were supported on a commercial premix flat burner (Howard et at. 1992) inside a variable pressure chamber as shown in Figure 1. The pressure chamber consisted of a stainless steel cylinder with an inside nominal diameter of 25 cm and a height of 40 cm which can be easily evacuated to less than 1 Torr using a 50-cfm direct drive vacuum pump with the pressure regulated with a baratron pressure gauge and controller. The burner consisted of a 6-cm diameter sintered stainless steel head with a surrounding bronze frit through which argon was flowed to form a protective shroud around the flame. The burner head was mounted on a motorized high-vacuum feedthrough flange which was coupled with an off-axis rotary feedthrough. The burner could be scanned vertically over more than 50 cm of travel with a precision of less than 50 micron and rotated with a precision of less than one half a degree. In addition, the burner was water cooled to maintain a constant temperature as measured by imbedded Alumel-Chromel thermocouples.

Under proper gas flow conditions the flame was one-dimensional with respect to the burner surface. In order to increase the spatial resolution the flame was operated at reduced pressure. Studies of low-pressure (or subatmospheric) flames have shown that the reaction zones expand with minimal distortion as pressure is reduced (Gaydon and Wolfhard 1949, Salmon and Laurendeau 1987). All of the flames in this report were operated at 20.0 Torr absolute pressure. Flow rates of C_2H_4, O_2 and Ar were 0.40, 1.2 and 2.8 standard liters/minute, respectively. Flow rates of H_2 and NO_2 were 3.25 and 1.60 standard liters/minute, respectively for total flow rates of approximately

4.5 liters/minute. The reactant gases were of commercial high-purity grade and were metered by mass flow controllers (calibrated with a wet test meter) and premixed in the burner prior to passing through the flat 6-cm diameter sintered stainless steel plug in the center of the burner surface.

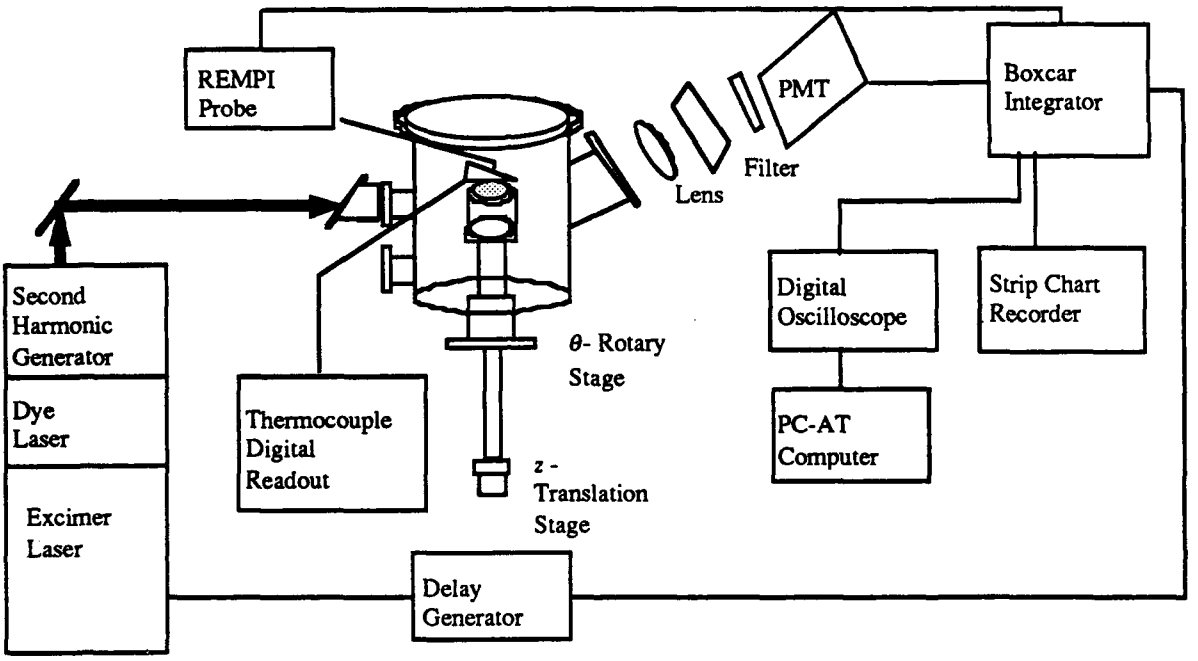

Figure 1. Schematic of Laser-Based and Thermocouple Diagnostics of the Experimental Apparatus.

Figure 1 also shows the schematic for the layout of the laser-based diagnostics. The excimer-pumped dye laser system equipped with a second harmonic generator (SHG) provided laser radiation both in the visible and ultraviolet. The pulse duration was approximately 10 nsec and the line width approximately 0.08 cm^{-1} for the dye laser and 0.16 cm^{-1} for the SHG. The laser beam was then focussed over the center of the burner with 50- to 100-cm focal length lenses. Light input to the chamber passed through Brewster angle windows in order to minimize light scattering. The Brewster windows also removed amplified stimulated emission (ASE) from the laser.

Laser-induced fluorescence was collected orthogonally to the excitation laser beam and focussed with a 300-mm focal length lens onto the image plane of the photomultiplier after passing an appropriate interference filter. The signal was then fed

into a boxcar integrator set for a 9-nsec gate (the short gate minimized the effect of collisional quenching and/or energy transfer of the rotationally excited states) and plotted on a strip-chart recorder or fed to a digital oscilloscope (500 MHz) and PC-type computer for recording. All LIF signals were obtained in the unsaturated regime, therefore, the laser probe energy was monitored by a photodiode and the resulting signal used to normalize the LIF signal.

The REMPI signal was collected by the optogalvanic probe as shown in Figure 2. It consisted of a 0.5-mm diameter platinum rod encased in a fused alumina tube for electrical insulation. One end of the rod was exposed to the flame in order to obtain signal. The focussed laser beam passed just below the exposed tip and would produce ions as the laser was scanned over the appropriate resonance wavelength. The charge was then detected as a voltage pulse across a 10 kΩ resistor connected between the probe and the negative bias voltage source (the anode for the circuit is the grounded burner). The resulting voltage pulses averaging a 15-μs decay lifetime were then amplified with a differential amplifier prior to processing by the boxcar integrator. Flame micophonics were minimized with bandpass (10 KHz to 1 MHz) filtering. The signal was then processed in like manner as the LIF signal.

Also essential to the operation of the REMPI probe was a low noise, low drift high-voltage power supply. To this end, a custom filter was added to a standard high-voltage power supply customarily used to supply photomultipliers. The filter consisted of a LC circuit as shown in Figure 3. The inductor was 10 Henry and each capacitor was 50 μFarad. This filter adequately smoothed any ripple and/or drift from the power supply.

Thermocouples were employed to obtain high quality, good resolution flame temperature profiles. The thermocouple consisted of 125-micron diameter platinum/platinum-10% rhodium wires spot welded together to form a junction and coated with a noncatalytic beryllium/yttrium oxide mixture (Kent 1970). As shown in Figure 4 the thermocouple wire was then spot welded to the opposing arms of a V-shaped probe, one arm of which was spring loaded to remove sag as the wire length changed with temperature. The thermocouple was also corrected for radiation loss by using a measured diameter of 190-micron for the coated thermocouple junction and 0.6

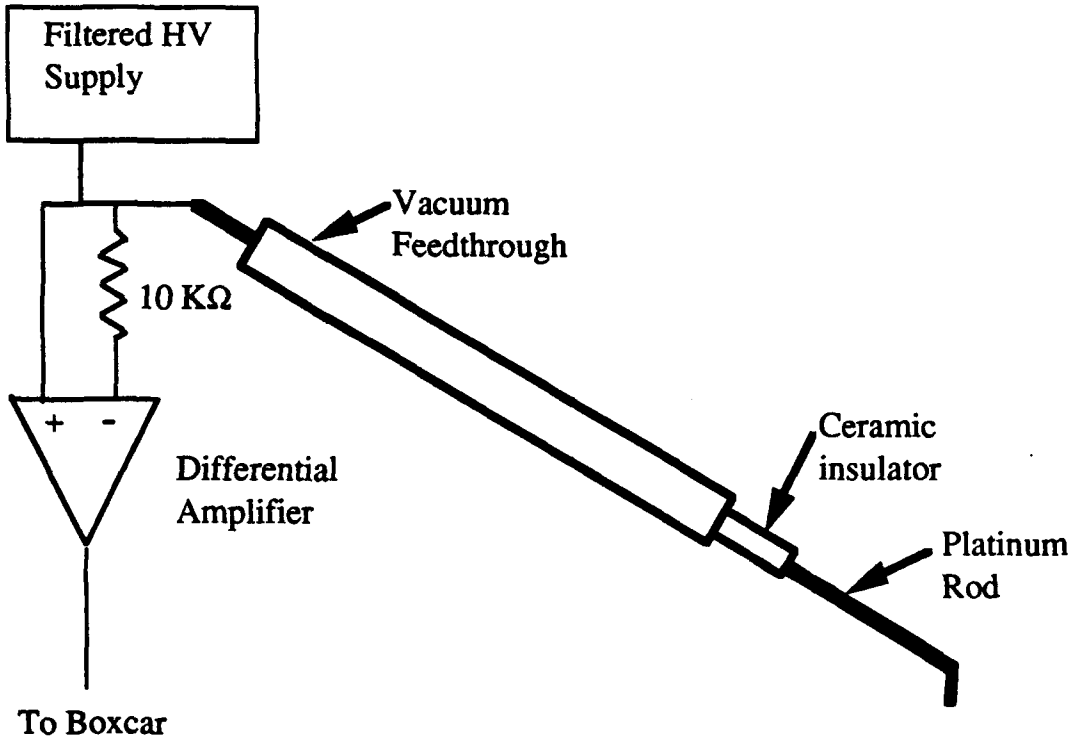

Figure 2. Schematic of REMPI Probe.

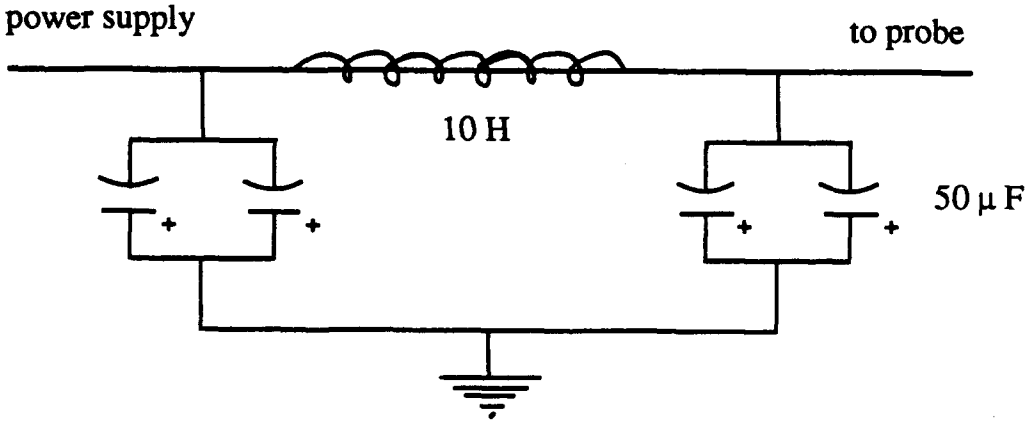

Figure 3. Schematic of REMPI Probe Bias Filter.

for the emissivity (Peterson 1981). Comparison with OH rotational LIF temperature measurements indicates an uncertainty of less than 50 K in the region of peak temperatures.

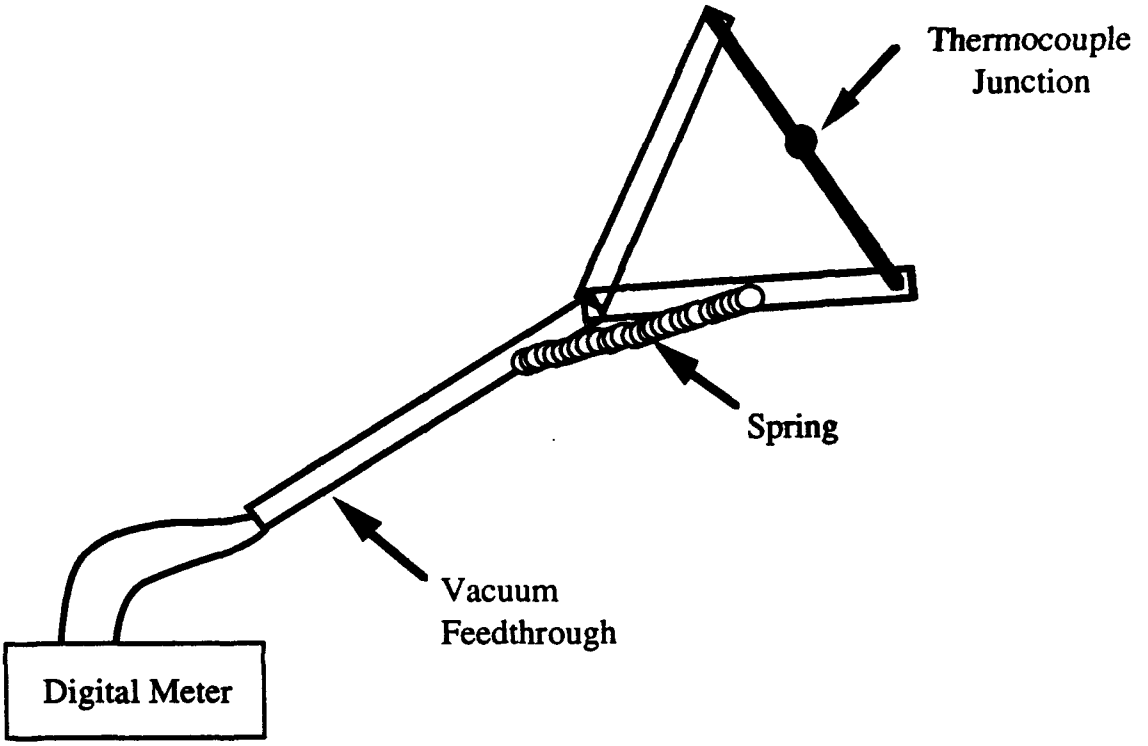

Figure 4. Schematic of Thermocouple Probe.

3. RESULTS AND DISCUSSION

3.1 Hydrocarbon Flames. Hydrocarbon skeletons provide the backbone for many of the fuels and propellants in use today. A discussion of propellant flames should therefore commence with discussion of the oxidation of hydrocarbons and the resulting heat and product formation.

3.1.1 Temperature Measurements. As mentioned in the Experimental Section, the thermocouples were corrected for radiation loss. Temperature correction from radiation loss by the thermocouple junction was approximated by equating the heat transferred to the thermocouple from the gases to that lost by radiation. The corrective term is given by (Hayhurst and Kittelson 1977, Peterson 1981)

$$\Delta T = T_{cal} - T_{obs} = \varepsilon\sigma d(T_{obs}^4 - T_o^4)/2k \qquad (1)$$

where ε is the emissivity of the coated thermocouple [taken to be 0.6 (Peterson 1981)], σ is the Stefan-Boltzmann constant, d is the diameter of the coated junction, T_o is approximately 300 K and k is the thermal conductivity of the gases present at the sampling region. This value was approximated with values for air since the correct proportions of gaseous reactants and products for a given temperature measurement were not known. Once the stable and transient species profiles are obtained a better approximation can be made. The uncertainty in temperature measurements was estimated to be 50 K in the region of peak temperature and 10 K in the preheat region.

Temperature measurements were also made by OH rotational spectroscopy. As this method is more time consuming than measurement by thermocouple, only spot checks by this method were made so as to compare results by the two methods. A rotational excitation spectrum of OH was obtained as shown in Figure 5. The spectrum corresponds to the excitation scheme in Table 1. The (1,0) band was chosen over the

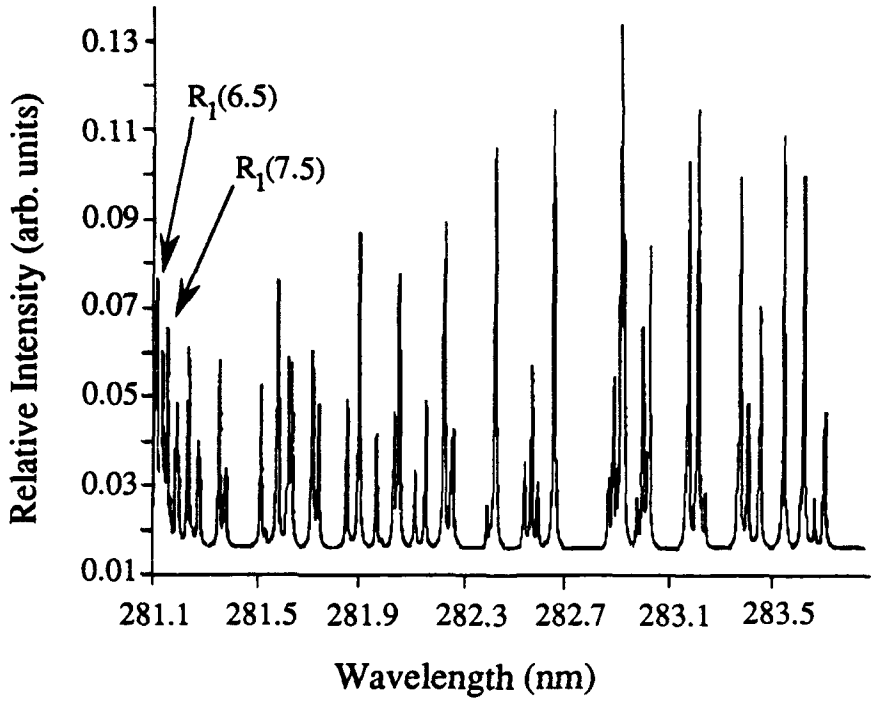

Figure 5. Observed and Simulated Rotational Spectra of the OH ($A\,^2\Sigma^+ - X\,^2\Pi$) (1,0) Band Near 281 nm for the $C_2H_4/O_2/Ar$ Flame at 20 Torr.

Table 1. Detection Schemes Employed for Species Profiling (LIF and REMPI)

Species	Excitation Wavelength	Transition	Emission Wavelength	Transition
OH	281 nm	$(A\ ^2\Sigma^+ \leftarrow X\ ^2\Pi_i)$ (1,0)	313 nm	(1,1) band
O	225.6 nm	$2p^3 3p\ ^3P \leftarrow 2p^4\ ^3P$	844.7 nm	$2p^3 3p\ ^3P \rightarrow 3s\ ^3S$
H	243 nm	$2s \leftarrow 1s$	N/A	(2+1) REMPI
CH_3	333 nm	$3p^2\ A_2 \leftarrow X^2\ A_2$	N/A	(2+1) REMPI
HCO	397 nm	$3p\ ^2\Pi(A'') \leftarrow X^2\ \Pi(A')$	N/A	(2+1) REMPI
NO_2	450 nm	$A^2\ B_1$ or $B^2\ B_2 \leftarrow X^2\ A_1$	540 nm	Unknown
NO	453 nm	$A\ ^2\Sigma^+ \leftarrow X\ ^2\Pi$ (0,0)	N/A	(2+2) REMPI

stronger (0,0) band near 306 nm in order to minimize self absorption. Intensity relationships can be distorted by self absorption and a thermal equilibrium might not be established. Temperatures within the laser focus then would not reflect the temperature of the surrounding gases.

The fluorescence intensity of several rotational lines as a function of laser energy indicated that the laser power was sufficiently attenuated for the one-photon process and that the experiments were operated in the unsaturated regime. This particular spectrum was taken near 6 mm in a stoichiometric $C_2H_4/O_2/Ar$ flame (see Figure 6 for temperature profile). Superimposed on the experimental data is a simulation of the corresponding LIF excitation spectrum. It is a result of fitting the experimental LIF spectrum with a spectral simulation based on a Boltzmann rotational energy distribution using multi-variable analysis (Anderson et al. 1982) of the observed spectra and known transition probabilities (Dimphl and Kinsey 1979) and molecular energy levels (Dieke and Crosswhite 1962). Other program variables include temperature, laser width, line position and pulse shape. Both Lorentzian and Gaussian functions were used to represent the laser line shape. As shown in Figure 6, the different line shapes change the simulation temperature by about 50 K with the Lorentzian function always producing the larger temperature. For the particular spectrum in Figure 5, the fitted spectrum is nearly identical with the experimental data. At this point the simulated fit indicates a rotational temperature of 1540 ±50 K which compares to 1550 ±20 K as measured by thermocouple. While the OH LIF

measurements agree well with the thermocouple measurements below 1800 K the comparison is more rough at higher temperatures. This difference is in part due to the fact that the OH LIF data were not corrected for the detector response (combined response of the intereference filter and the photomultiplier).

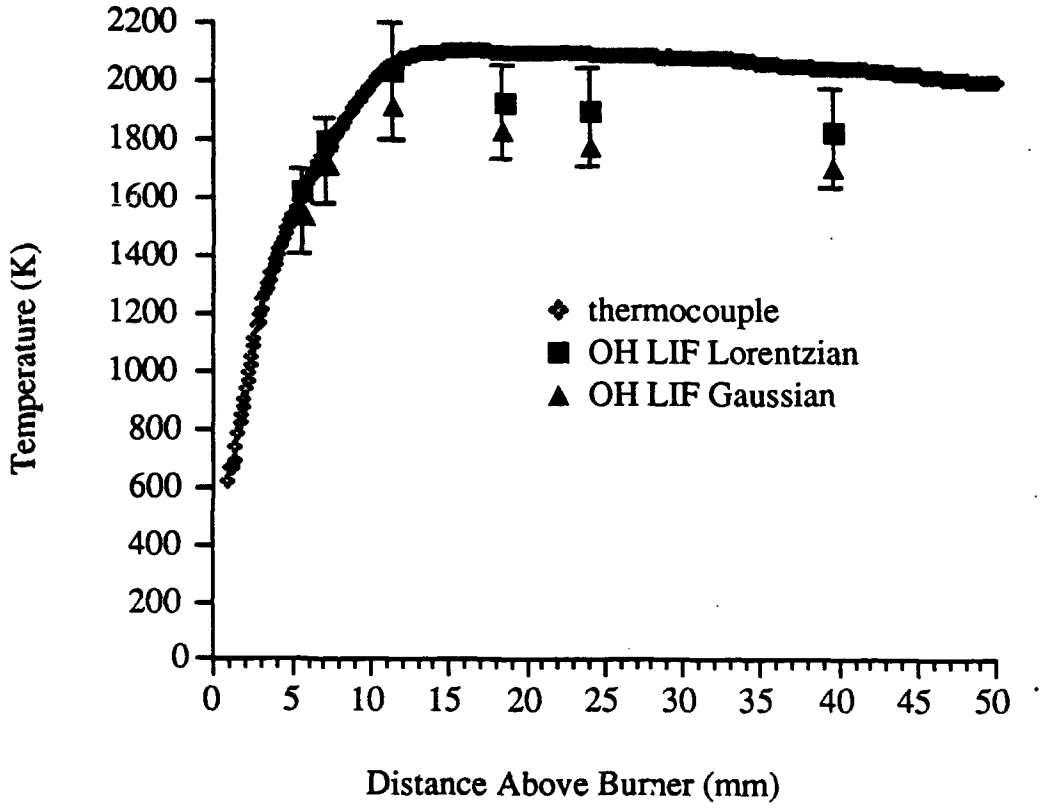

Figure 6. Temperature Profiles of Stoichiometric $C_2H_4/O_2/Ar$ Flame at 20 Torr.

In addition to the comparison in Figure 6 of the thermocouple data with that obtained by OH LIF rotational spectroscopy, the higher resolution thermocouple data begin to give indications of the flame structure in this flame. Firstly, the flame just above the burner surface is hotter (600 K) than the burner as indicated by imbedded thermocouples (320 K). The temperature difference can be due to several variables that include low thermal conductivity of the sintered frit and a small to moderate degree of stabilization of the flame by the burner. The region of large thermal gradient from 0 to 5 mm is indicative of the preheat region. From here to the region of maximum temperature is contained the reactive zone. It is also delineated by the zone of visibly radiating species (luminous zone). Above the region of maximum temperature is the

burnt gas region. Reactions are nearing completion and again the flame is nonradiative in the visible. A slight decrease in temperature is noted in this region. It is essentially due to radiative losses from the flame. If the profile decreased rapidly, turbulance and mixing of gases cooled by contact with the chamber walls would be indicated. Such a decrease would therefore be indicative of loss of one-dimensionality in the flame. However, the profile decreases evenly and slowly and thereby it is inferred that the flame is one-dimensional to well above 50 mm above the burner surface.

3.1.2 Spectroscopic Profile Measurements. The different optical spectroscopic diagnostics used are given in Table 1. The relative (normalized to unity) concentration profiles were obtained by monitoring the intensities of rotational transitions relatively insensitive to temperature variations. These transitions were calculated by the following relation (Eckbreth 1988):

$$J^2 + J - (k_B/hcB_v)T_{av} = 0 \qquad (2)$$

where J is the rotational level, k_B, h, c, B_v are spectroscopic constants and T_{av} the average flame temperature. For example, it was determined that for OH LIF that both the J = 6.5 and 7.5 lines of the R_1 branch of the (0,1) transition could be monitored and found to give equivalent results and for O-atom LIF, the J = 2 excitation line of the ground state could be monitored.

In conjunction with the experimental profiles, the Sandia National Laboratory premix laminar flow flame codes (Kee et al. 1985) have been utilized to model the $C_2H_4/O_2/Ar$ low-pressure flame in order to better understand the detailed chemistry. The mechanism employed in the following simulations is that of Miller and Bowman (Miller and Bowman 1989). The model was operated in the burner-stabilized flame mode with the experimental temperature profile in Figure 6 as input to the calculation. The resulting concentration profiles, normalized to unity, are presented with the experimental data (also normalized to unity) in Figures 7 and 8. Comparison between the experimental and calculated profiles shows several profiles that agree well. Of these, O-atom shows the best agreement through the preheat and reactive zones. The OH profiles, while the model is delayed relative to the experimental, agree in the shape and even the small peak occurring at less than 5 mm.

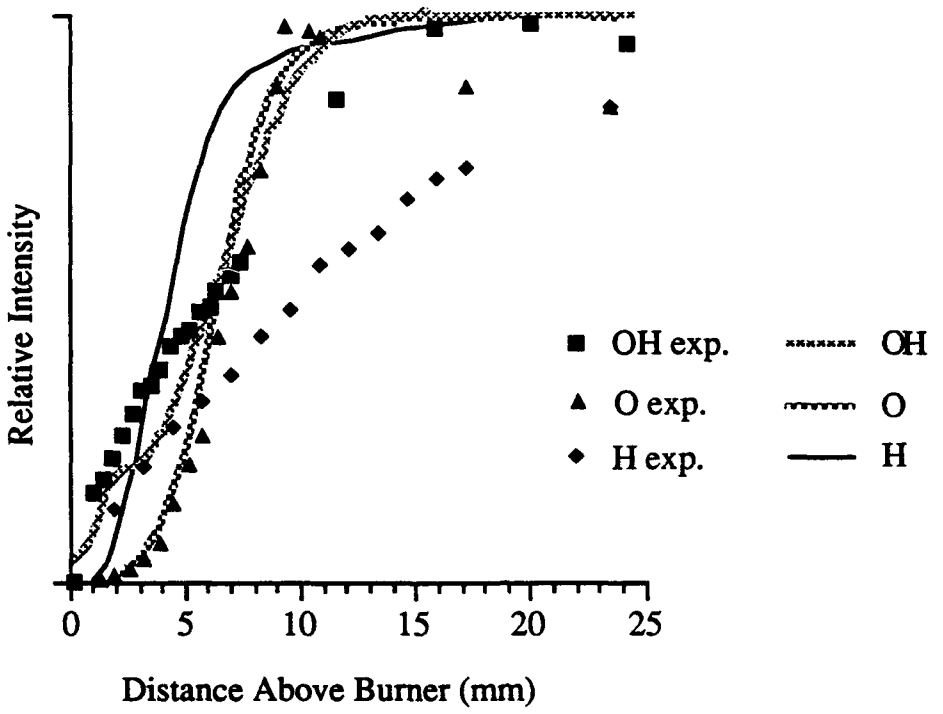

Figure 7. Theoretical and Experimental OH, O and H Profiles of Stoichiometric $C_2H_4/O_2/Ar$ Flame at 20 Torr.

The feature in the OH profile may be attributed to competition between the high temperature formation of OH via the following chain-branching reactions,

$$H + O_2 \rightarrow O + OH \quad (3)$$

and

$$O + H_2 \rightarrow H + OH \quad (4)$$

with the three body reactions of

$$H + O_2 + M \rightarrow HO_2 + M \quad (5)$$

and

$$HO_2 + H + M \rightarrow 2OH + M \quad (6)$$

which are favored at lower temperature (Warnatz 1978).

There is some discrepancy in the burnt gas region of the O-atom profile and its corresponding simulation. The O-atom LIF (2-photon) profile was determined under high photon flux conditions so as to minimize quenching effects. However, high

photon flux may lead to photochemical perturbation of the sampled volume. In addition, it is possible that O-atom LIF results in this region may have been affected by a recently recognized phenomenon that is specific to three-level systems such as O-atom two-photon LIF, namely, amplified spontaneous emission (ASE) (Alden et al. 1989). In this situation, a population inversion can be created between the two-photon pumped $2p^3 3p\ ^3P$ upper state and the lower $3s\ ^3S$ state to which it fluoresces such that the normal LIF signal will be depleted in favor of ASE signal which will be emitted along the direction of the incident laser beam and not collected by the detector. The ASE potential problem should be a function of total O-atom population as well as of laser pump energy, which would argue that it would be greater in the flame zone region (where O-atom concentrations are highest) rather than in the preheat region. This is what is observed at distances greater than 12 mm.

Methyl radical may be generated by the following reactions (Vandooren et al. 1986, Hucknall 1985):

$$C_2H_4 + OH \rightarrow H_2CO + CH_3 \quad (7)$$

$$C_2H_4 + O \rightarrow H + C_2H_3O \quad (8)$$

$$C_2H_4 + O \rightarrow CH_3 + HCO \quad (9)$$

where C_2H_3O may decompose to CH_3 and CO, or further react with O to yield CH_3 and CO_2. The existance of HCO in this flame, as shown in Figure 8, suggests that Reaction 8 plays little, if any, role in the formation of CH_3 radicals in the above mechanism. Reaction 9 implies a simultaneous formation of the HCO and CH_3 radicals and is not consistent with our results which show that the HCO is formed subsequent to the CH_3 radical. The delayed peaking in the radicals in Figure 8 can be explained by Reaction 7 which is known to occur at low temperatures followed by formation of HCO by (Vandooren et al. 1986),

$$CH_3 + O \rightarrow H_2CO + H \quad (10)$$

and

$$H_2CO + R \rightarrow HCO + RH \quad (11)$$

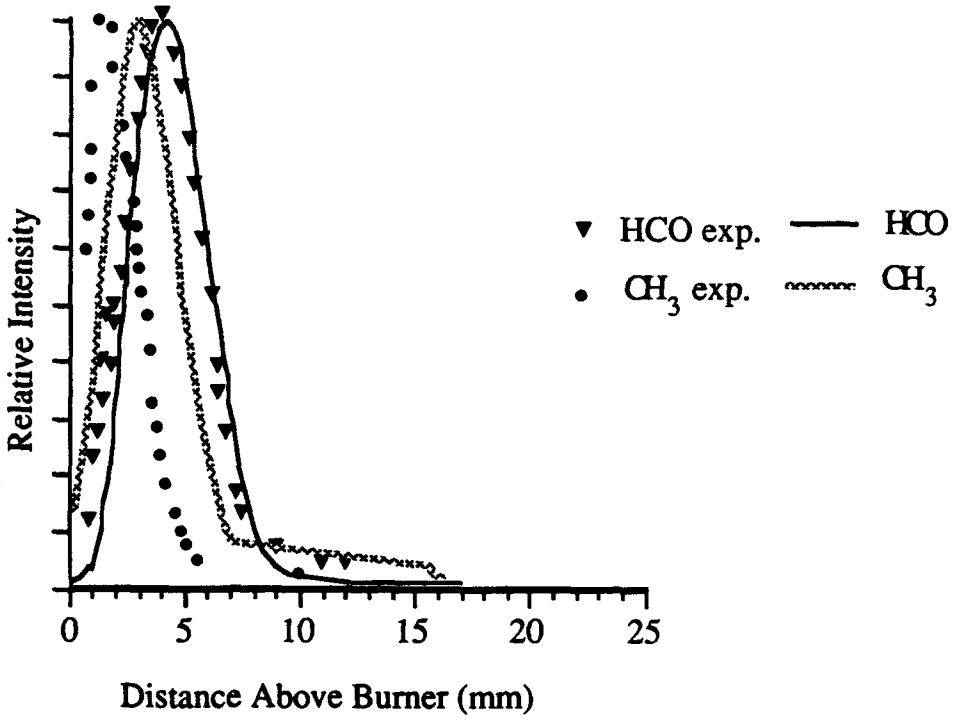

Figure 8. Theoretical and Experimental HCO and CH_3 Profiles of Stoichiometric $C_2H_4/O_2/Ar$ Flame at 20 Torr.

where R is O, H, or OH. However, at temperatures below 600-700 K and pressures above a few Torr, it has been shown (Tully 1988) that the addition reaction of OH to ethylene followed by adduct stabilization,

$$C_2H_4 + OH \rightarrow C_2H_4OH^* \rightarrow C_2H_4OH + M \ , \qquad (12)$$

dominates over Reaction 7. However, at higher temperatures the reaction

$$C_2H_4 + OH \rightarrow C_2H_3 + H_2O \qquad (13)$$

is important (Baldwin and Walker 1980). C_2H_3 can further react with O_2 to form H_2CO and HCO (Slagle et al. 1984). It is this reaction as well as Reaction 7 that provides an efficient route for HCO formation.

Further discrepancy with the model is observed in that the model profiles of HCO and CH_3 are delayed relative to the experimental results (see Figure 8). While the difference is only about 1 mm for HCO, the CH_3 profiles are separated by more than 3 mm. For reactions occurring in the preheat region where the thermal gradients are not

that large, a difference of 3 mm is significant. It is likely that these differences can explain part of the later discrepancies with the OH and H-atom profiles. However, they can not explain fully the difference between profiles for H-atom. The REMPI technique for H-atom detection is being further evaluated for possible interferences that could account for the difference.

3.2 Nitrogen Chemistry. Nitrogen oxides form an important class of oxidizers that are added to hydrocarbon skeleton backbones to create effective propellants. One of the simplest flames, from a chemical standpoint, to describe utilization of nitrogen oxides is the oxidation of hydrogen by nitrogen dioxide forming nitrogen gas and water vapor. Argon was not added to dilute the flame since the preheat and luminous zones were sufficiently expanded at 20 Torr for adequate spatial resolution. At present, modelling efforts have not successfully described the flame and only the experimental results will be discussed.

3.2.1 Temperature Measurements. Figure 9 contains the temperature profiles as measured by thermocouple from three flames: (1) fuel rich with Φ (defined as the

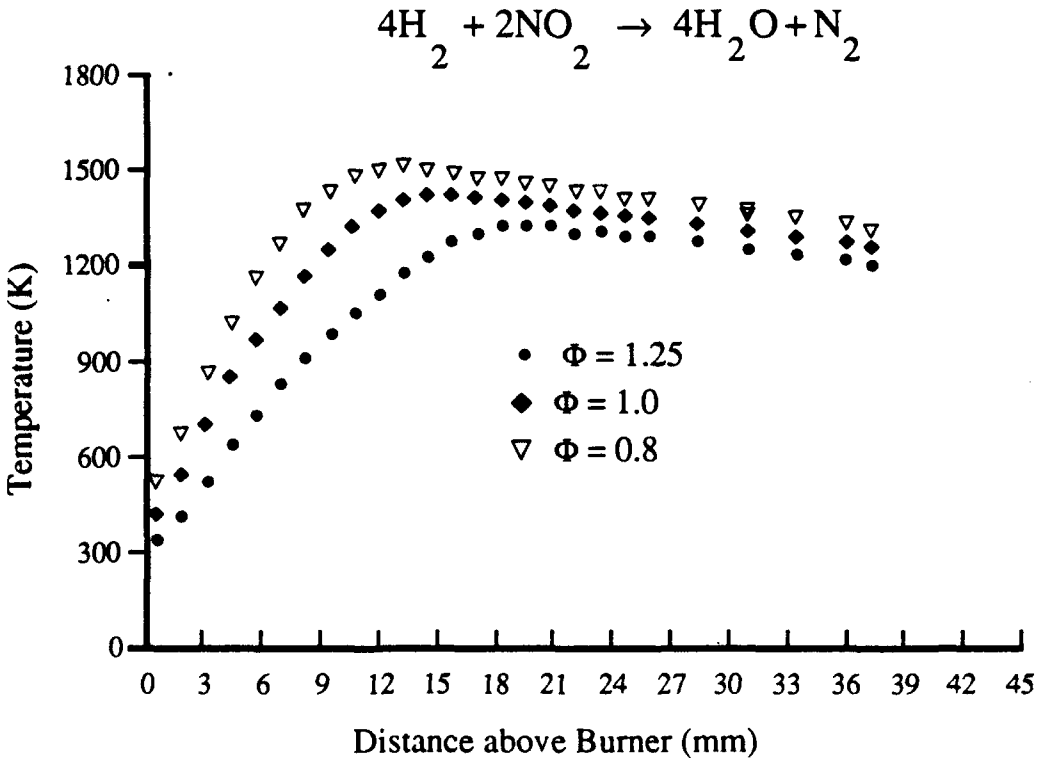

Figure 9. Temperature Profiles of H_2/NO_2 Flames at 20 Torr.

ratio of fuel to oxidizer divided by the stoichiometric ratio) of 1.3, (2) stoichiometric with Φ of 1.0 and (3) fuel lean with Φ of 0.8. Of the three, the stoichiometric flame was considered for further study by laser diagnostics. Temperature measurements were also made with OH LIF. However, the simulated temperatures were all much higher that those measured by thermocouple. Since the same thermocouple was used for these measurements as for those successfully obtained and compared with OH measurements in Section 3.1, it was inferred that that the laser was affecting the local temperature at the focal point and registering a temperature that is too high. Looking at the OH excitation spectrum in Figure 10 taken 4.2 mm above the burner, it is apparent that the measurement is not as good as for the ethylene/oxygen flame in Section 3.1 even though all operating conditions were the same excepting the flame. Since NO_2 is easily photolyzed and is in abundance at this point in the flame (photolysis products would elevate the local temperature), this result is not completely surprising. Therefore another laser-based thermometer operating at longer wavelengths (lower photon energy) would be beneficial for this portion of the flame.

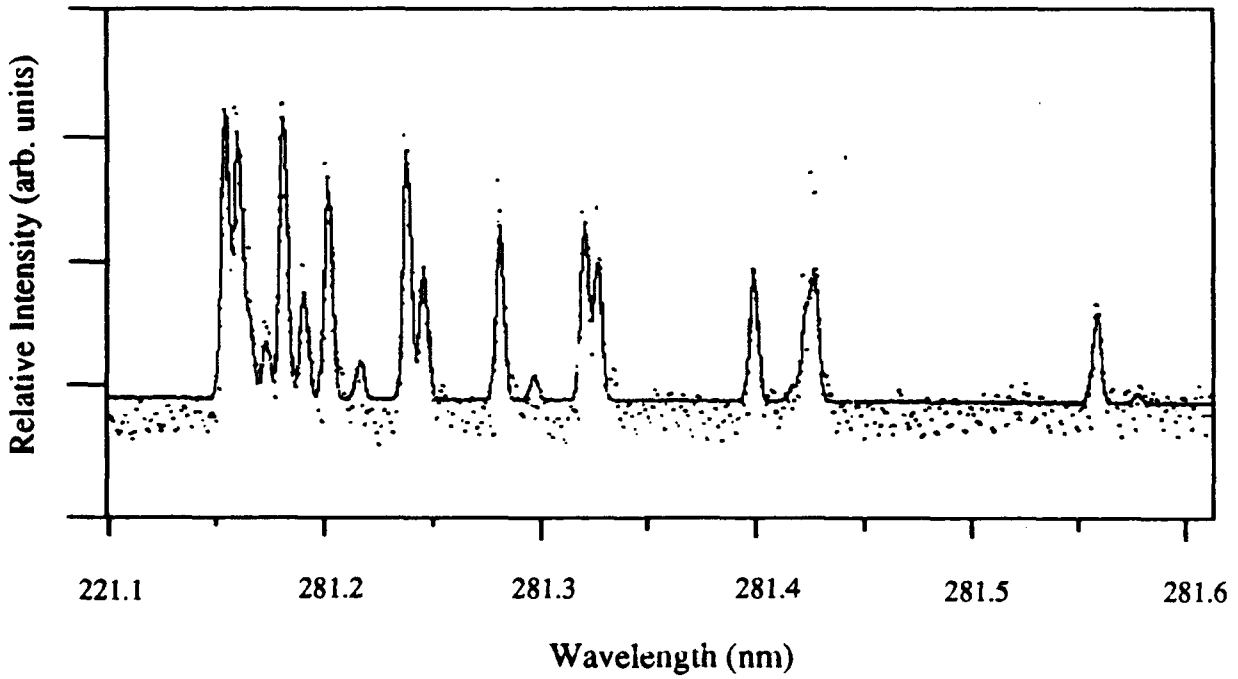

Figure 10. Observed and Simulated Spectra of OH in H_2/NO_2 Flame at 20 Torr. Simulation Temperature of 1039 ±100 K.

It was expected that NO as generated by

$$NO_2 + M \rightarrow NO + O + M \quad (14)$$

or by

$$NO_2 + R \rightarrow NO + RO \quad (15)$$

where R represents H, O, or OH would be abundant in this flame. The longer wavelength, 453 nm versus 281 nm for OH, should remove some in the perturbation problems. The detection scheme for NO is given in Table 1 and further elucidated in

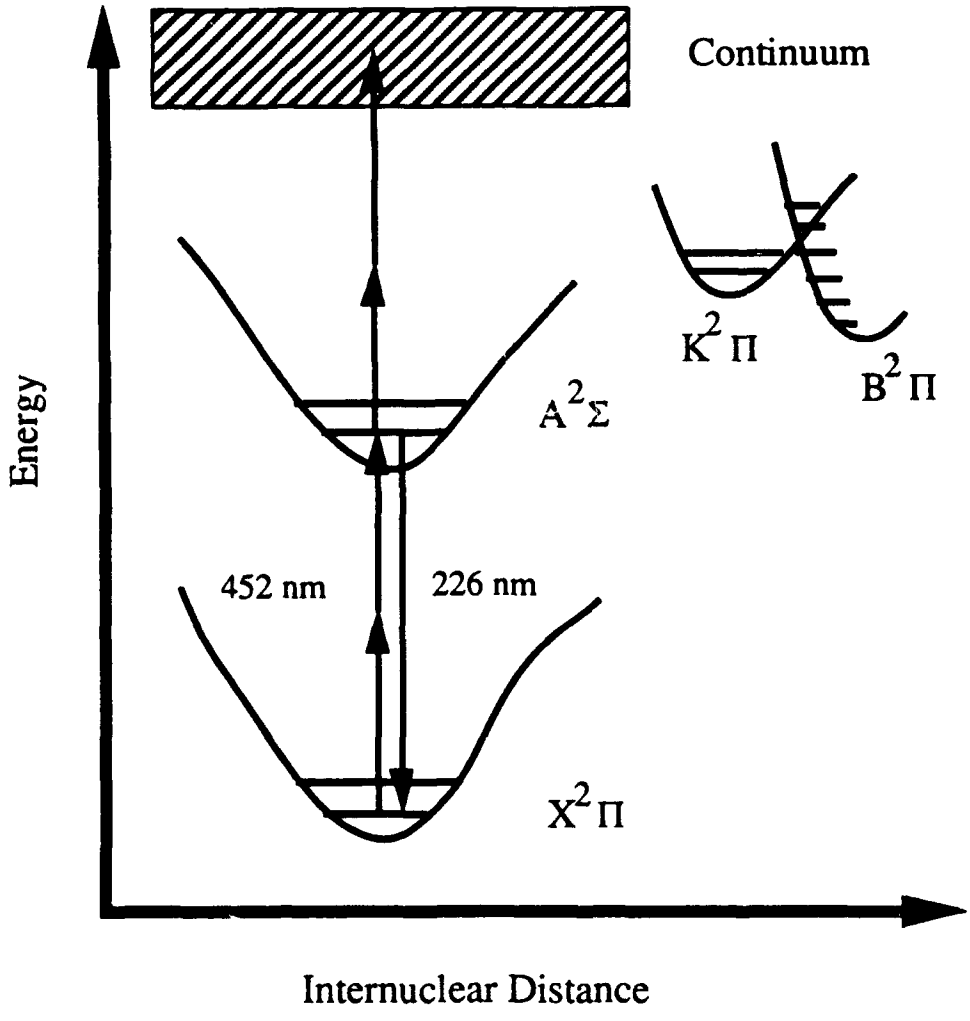

Figure 11. Potential Energy Surfaces for REMPI of NO.

Figure 11. Figure 11 describes the potential energy surfaces accessed in the proposed REMPI detection. In this technique two photons are absorbed thus promoting the molecule from the ground state manifold to the corresponding A state. From this intermediate state, two more photons are rapidly absorbed and an electron is ejected from the molecule thus forming a positive ion. This process occurs sufficiently fast that intramolecular transitions do not occur from the intermediate state manifold and the ion is formed with the original rotational energy signature. This diagnostic gave reasonable results for the concentration profile and so the same REMPI technique was tried as a thermometer. Preliminary results at room temperature, as shown in Figure 12, indicated that the technique should be usable. However, once in the flame,

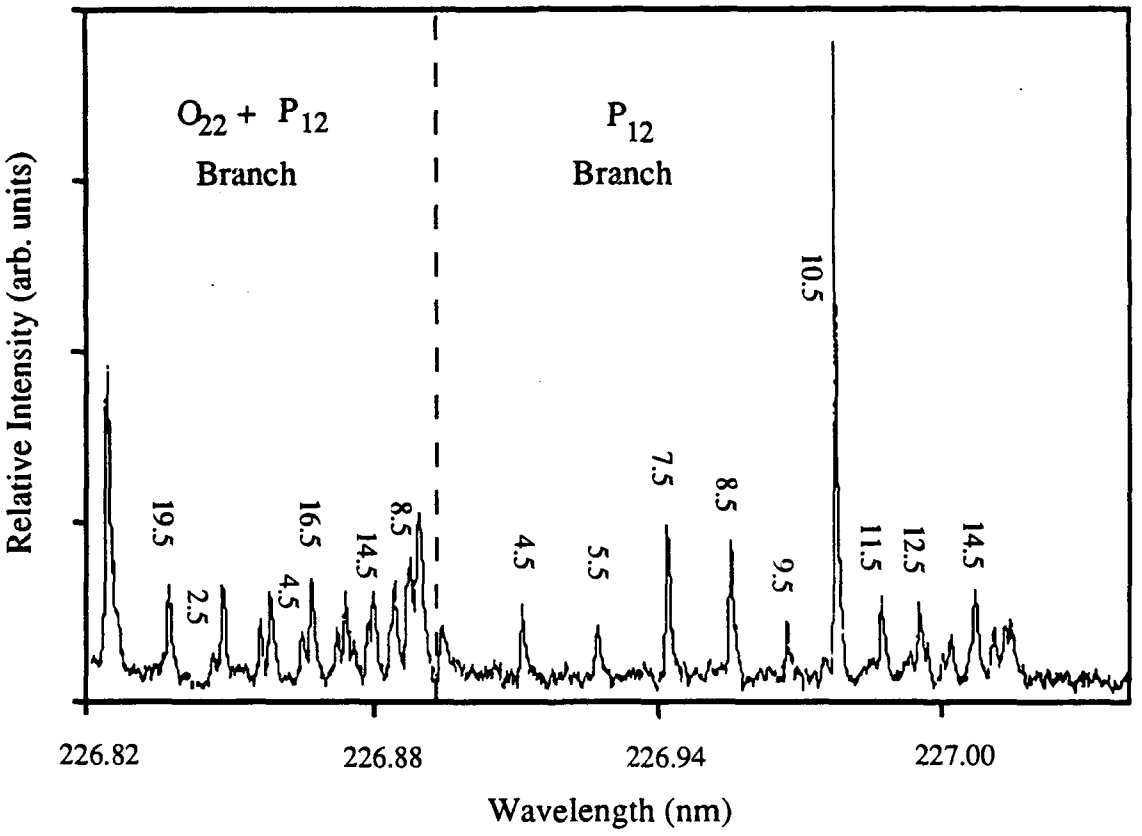

Figure 12. REMPI Excitation Spectrum of NO at 20 Torr at Room Temperature.

reasonable temperatures were only obtained up to moderate temperatures near 1000 K. Several suggestions were offerred to account for this behavior. First, as noted in Figure 13, a portion of Figure 12 near 320 K, as the rotational progression increases,

the simulated and experimental peaks begin to diverge as to line position. As the divergence appears to be monotonic with ΔJ values, it would appear that the rotational constants as currently cataloged are not fully correct. As the transitions are not as well-known as those of OH, it is possible that the simulation does not adequately represent the experimental spectrum. It is also possible that competing multiphoton processes are affecting the local flame temperature at the laser focus since room temperature measurements of NO are quite successfull. Another possibility is that the REMPI probe affects the probed volume above a threshold temperature. The investigation for a suitable laser-based thermometer is still underway.

3.2.2 Concentration Profiles. The two most important nitrogen carriers easily accessable by laser in this flame are NO and NO_2. Their detection and profile measurement were done using the detection schemes in Table 1. An excitation spectrum of NO is shown in Figure 12 (room temperature), a similar LIF profile for NO_2 was not generated since it exhibits a broad band emission near 540 nm. For measurement of NO_2, a broad band monochromator replaced the usual interference

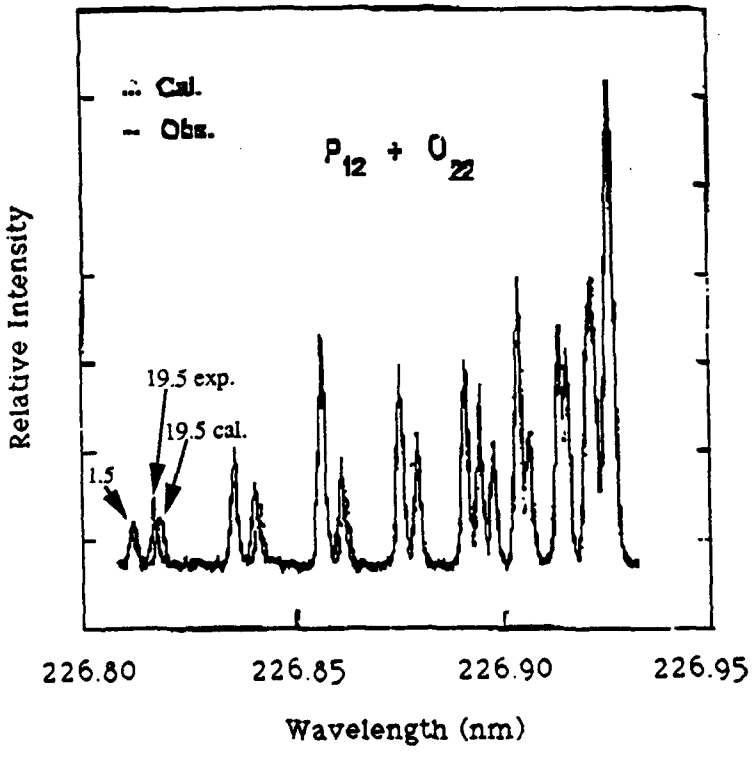

Figure 13. Observed and Simulated REMPI Spectrum for NO in H_2/NO_2 Flame at 20 Torr.

filter and the emission collected at 540 nm for all measurements. As shown in Figure 14, in the flame NO_2 is rapidly consumed and is exhausted in the luminous zone near 8 mm above the burner. NO back diffuses to the burner surface, increases to a maximum in the luminous zone and then rapidly diminishes and achieves low levels prior to 18 mm above the surface. Also implied in the figure is an intimate connection between OH and NO. Both of the profiles have the same shape and spatial location in the flame. Such a connection implies that the mechanism for production of NO is likely Reaction 14 rather than Reaction 13. The full mechanism would also need to effectively utilize NO and OH in the upper limits of the preheat zone and the lower region of the luminous zone. Of interest would be the concentration profiles of H-atom, O-atom and H_2, several of which are not not obtainable with the current apparatus using the current laser-based diagnostics with this flame. Other techniques such as molecular-beam sampling would be needed to obtain a full survey of major and minor species in the flame.

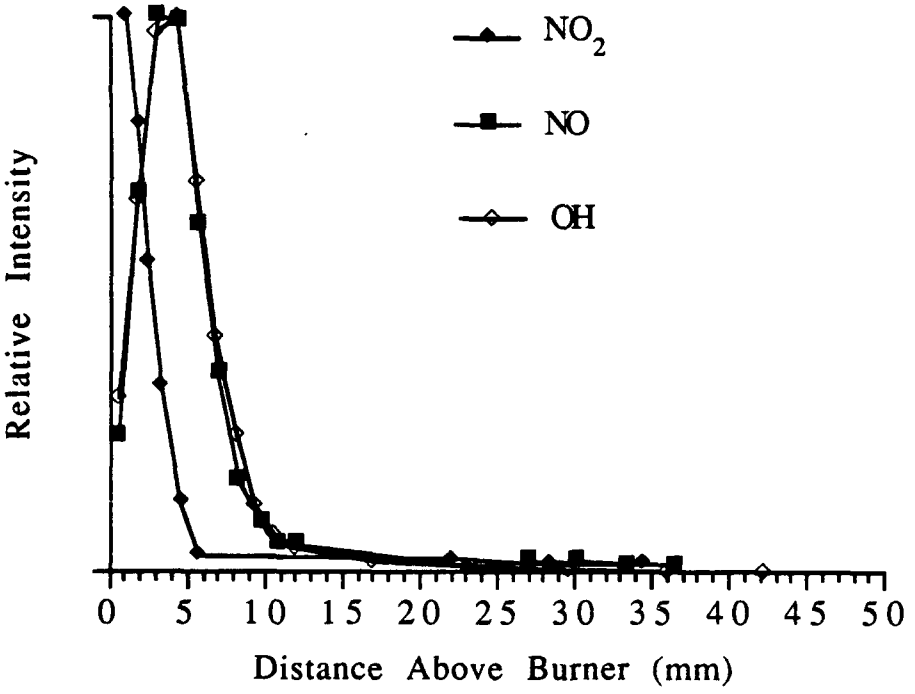

Figure 14. Species Profiles for OH, NO and NO_2 in H_2/NO_2 Flame at 20 Torr.

4. SUMMARY

A major research facility consisting of a low-pressure burner apparatus has been constructed at the Ballistic Research Laboratory for the purpose of studying the detailed flame chemistry relevant to the gaseous flames of burning propellants. Temperature and species profiles were obtained for $C_2H_4/O_2/Ar$ and H_2/NO_2 flames at 20 Torr. The temperature profiles were obtained with Pt/Pt-Rh(10%) thermocouples coated with an inert beryllium/yttrium oxide. OH LIF rotational spectroscopy employing the ($A\ ^2\Sigma^+ - X\ ^2\Pi_i$) (1,0) band near 281 nm was also utilized for temperature measurements. The temperatures were abstracted from a spectral simulation based on a Boltzmann energy distribution and compared to those obtained by coated thermocouples. In the case of the $C_2H_4/O_2/Ar$ flame, the temperature profile was used as input data for the Sandia National Laboratories one-dimensional premixed laminar flame code to generate species profiles. The O, OH, CH_3 and HCO species profiles which were obtained spectroscopically by laser-induced fluorescence and/or resonance-enhanced multiphoton ionization techniques agree well with those generated by the model. For the H_2/NO_2 flame, LIF profiles of OH and NO_2 were obtained as well as a REMPI of NO. A second thermometry technique for this flame utilizing NO REMPI was attempted and appears to work only at temperatures below 1000 K.

5. REFERENCES

Alden, M., Westblom, U. and Goldsmith, J. E. M., Opt. Lett., Vol. 14, p. 305, 1989.

Anderson, W. R., Decker, L. J., and Kotlar,A. J., Combust. Flame, Vol. 48, p. 163, 1982.

Baldwin, R. R. and Walker, R. W., Eighteenth Symposium (Int.) on Combustion, p. 819, The Combustion Institute, 1980.

Cattolica, R. J. and Mataga, T. G., Chem. Phys. Lett., Vol. 182, p. 623, 1991.

Dieke, G. H. and Crosswhite, H. M., J. Quant. Spectrosc. Radiat. Transfer, Vol. 2, p. 97, 1962.

Dimpfl, W. L. and Kinsey, J. L., J. Quant. Spectrosc. Radiat. Transfer, Vol. 21, p. 233, 1979.

Eckbreth, A. C., Laser Diagnostics for Combustion Temperature and Species, Abacus, Cambridge; 1988.

Gaydon, A. G. and Wolfhard, H. G., Third Symposium (Int.) Combustion and Explosion Phenomena, Williams & Wilkins, Baltimore 1949; p. 504.

Goldsmith, J. E. M., J. Chem. Phys., Vol 78, p. 1610, 1983.

Hayhurst, A. N. and Kittelson, D. B., Combust. Flame, Vol. 28, p. 301, 1977.

Howard, S. L., Newberry, J. E., Sausa, R. C., and Miziolek, A. W., BRL Report, BRL 3333, 1992.

Hucknall, D. J., Chemistry of Hydrocarbon Combustion, Chapman and Hall, New York; 1985.

Kee, R. J., Grcar, J. F., Smooke, M. D., and Miller, J. A., Sandia National Laboratories Report, SAND85-8240, 1985.

Kent, J. H., Combust. Flame, Vol. 14, p. 279, 1970.

Lucht, R. P., Salmon, J. T., King, G. B., Sweeney, D. W., and Laurendeau, N. M., Optics Lett., Vol. 8, p. 365, 1983.

Miller, J. A. and Bowman, C. T., Prog. Energy Combust. Sci., Vol. 15, p. 287, 1989.

Peterson, R. C., PhD Thesis, Purdue University, 1981.

Salmon, J. T. and Laurendeau, N. M., Applied Optics, Vol. 26, p. 2881, 1987.

Slagle, I. R., Park, J. Y., Heaven, M. C., and Gutman D., J. Am. Chem. Soc., Vol. 106, p. 4356, 1984.

Vandooren, J., Oldenhove, L., and Van Tiggelen, P. T., Combust. Flame, Vol. 64, p. 127, 1986.

INTENTIONALLY LEFT BLANK

No. of Copies	Organization
2	Administrator Defense Technical Info Center ATTN: DTIC-DDA Cameron Station Alexandria, VA 22304-6145
1	Commander U.S. Army Materiel Command ATTN: AMCAM 5001 Eisenhower Ave. Alexandria, VA 22333-0001
1	Commander U.S. Army Laboratory Command ATTN: AMSLC-DL 2800 Powder Mill Rd. Adelphi, MD 20783-1145
2	Commander U.S. Army Armament Research, Development, and Engineering Center ATTN: SMCAR-IMI-I Picatinny Arsenal, NJ 07806-5000
2	Commander U.S. Army Armament Research, Development, and Engineering Center ATTN: SMCAR-TDC Picatinny Arsenal, NJ 07806-5000
1	Director Benet Weapons Laboratory U.S. Army Armament Research, Development, and Engineering Center ATTN: SMCAR-CCB-TL Watervliet, NY 12189-4050
(Unclass. only) 1	Commander U.S. Army Rock Island Arsenal ATTN: SMCRI-TL/Technical Library Rock Island, IL 61299-5000
1	Director U.S. Army Aviation Research and Technology Activity ATTN: SAVRT-R (Library) M/S 219-3 Ames Research Center Moffett Field, CA 94035-1000
1	Commander U.S. Army Missile Command ATTN: AMSMI-RD-CS-R (DOC) Redstone Arsenal, AL 35898-5010

No. of Copies	Organization
1	Commander U.S. Army Tank-Automotive Command ATTN: ASQNC-TAC-DIT (Technical Information Center) Warren, MI 48397-5000
1	Director U.S. Army TRADOC Analysis Command ATTN: ATRC-WSR White Sands Missile Range, NM 88002-5502
1	Commandant U.S. Army Field Artillery School ATTN: ATSF-CSI Ft. Sill, OK 73503-5000
(Class. only) 1	Commandant U.S. Army Infantry School ATTN: ATSH-CD (Security Mgr.) Fort Benning, GA 31905-5660
(Unclass. only) 1	Commandant U.S. Army Infantry School ATTN: ATSH-CD-CSO-OR Fort Benning, GA 31905-5660
1	WL/MNOI Eglin AFB, FL 32542-5000
	Aberdeen Proving Ground
2	Dir, USAMSAA ATTN: AMXSY-D AMXSY-MP, H. Cohen
1	Cdr, USATECOM ATTN: AMSTE-TC
3	Cdr, CRDEC, AMCCOM ATTN: SMCCR-RSP-A SMCCR-MU SMCCR-MSI
1	Dir, VLAMO ATTN: AMSLC-VL-D
10	Dir, USABRL ATTN: SLCBR-DD-T

No. of Copies	Organization
4	Commander U.S. Army Research Office ATTN: R. Ghirardelli D. Mann R. Singleton R. Shaw P.O.Box 12211 Research Triangle Park, NC 27709-2211
2	Commander U.S. Army Armament Research, Development, and Engineering Center ATTN: SMCAR-AEE-B, D. S. Downs SMCAR-AEE, J. A. Lannon Pinatinny Arsenal, NJ 07806-5000
1	Commander U.S. Army Armament Research, Development, and Engineering Center ATTN: SMCAR-AEE-BR, L. Harris Pinatinny Arsenal, NJ 07806-5000
1	Office of Naval Research Department of the Navy ATTN: R. S. Miller, Code 432 800 N. Quincy Street Arlington, VA 22217
5	Commander Naval Research Laboratory ATT: M. C. Lin J. McDonald E. Oran J. Shnur R. J. Doyle, Code 6110 Washington, DC 20375
1	Superintendent Naval Postgraduate School Dept. of Aeronautics ATTN: D. W. Netzer Monterey, CA 93940
1	AFOSR ATTN: J. M. Tishkoff Bolling Air Force Base Washington, DC 20332
1	NASA Langley Research Center Langley Station ATTN: G. B. Northam/MS 168 Hampton, VA 23365

No. of Copies	Organization
1	Aerojet Solid Propulsion Co. ATTN: P. Micheli Sacramento, GA 95813
1	Applied Combustion Technology, Inc. ATTN: A. M. Varney P. O. Box 607885 Orlando, FL 32860
1	University of California Los Alamos Scientific Laboratory P. O. Box 1663, Mail Stop B216 Los Alamos, NM 87545
1	AVCO Everett Research Laboratory Division ATTN: D. Stickler 2385 Revere Beach Parkway Everett, MA 02149
1	Battelle ATTN: TACTEC Library, J. Huggins 505 King Avenue Columbus, OH 43201-2693
1	University of Texas Department of Chemistry ATTN: W. Gardner Austin, TX 78712
1	Exxon Research & Eng. Co. ATTN: A. Dean Route 22E Annandale, NJ 08801
1	General Applied Science Laboratories, Inc. 77 Raynor Avenue Ronkonkama, NY 11779-6649
1	General Electric Ordnance Systems ATTN: J. Mandzy 100 Plastics Avenue Pittsfield, MA 01203
1	General Motors Rsch Labs Physical Chemistry Department ATTN: T. Sloane Warren, MI 48090-9055
2	Hercules, Inc. Allegheny Ballistics Lab. ATTN: W. B. Walkup E. A. Yount P. O. Box 210 Rocket Center, MV 26726

No. of Copies	Organization
1	Alliant Techsystems, Inc. ATTN: R. E. Tompkins MN38-3300 5700 Smetana Drive Minnetonka, MN 55343
3	Pennsylvania State University Applied Research Laboratory ATTN: K. K. Kuo H. Palmer M. Micci University Park, PA 16802
1	IIT Research Institute ATTN: R. F. Remaly 10 West 35th Street Chicago, IL 60616
2	Director Lawrence Livermore National Laboratory ATTN: C. Westbrook M. Costantino P. O. Box 808 Livermore, CA 94550
1	Lockheed Missiles & Space Co. ATTN: George Lo 3251 Hanover Street Dept. 52-35/B204/2 Palo Alto, CA 94304
1	Director Los Alamos National Lab ATTN: B. Nichols, T7, MS-B284 P. O. Box 1663 Los Alamos, NM 87545
1	Olin Ordnance ATTN: V. McDonald, Library P. O. Box 222 St. Marks, FL 32355-0222
1	Paul Gough Associates, Inc. ATTN: P. S. Gough 1048 South Street Portsmouth, NH 03801-5423
2	Princeton Combustion Research Laboratories, Inc. ATTN: M. Summerfield N. A. Messina 475 US Highway One Monmouth, Junction, NJ 08852
1	Hughes Aircraft Company ATTN: T. E. Ward 8433 Fallbrook Avenue Canoga Park, CA 91303

No. of Copies	Organization
2	Rockwell International Corp. Rocketdyne Division ATTN: T. L. Bunn J. E. Flanagan/HB02 6633 Canoga Avenue Canoga Park, CA 91303
1	Dow Chemical U.S.A. Analytical Sciences, Thermal Group ATTN: S. W. Froelicher 1897 Building Midland, Michigan 48667
4	Director Sandia National Laboratories Division 8354 ATTN: R. Cattolica S. Johnston P. Mattern D. Stephenson Livermore, CA 94550
1	Science Applications, Inc. ATTN: R. B. Edelman 23146 Cumorah Crest Woodland Hills, CA 91364
3	SRI International ATTN: G. Smith D. Crosley D. Golden 333 Ravenswood Avenue Menlo Park, CA 94025
1	Stevens Institute of Tech. Davidson Laboratory ATTN: R. McAlevy, III Hoboken, NJ 07030
1	Sverdrup Technology, Inc. LeRC Group ATTN: R. J. Locke, MS SVR-2 2001 Aerospace Parkway Brook Park, OH 44142
1	Thiokol Corporation Elkton Division ATTN: S. F. Palopoli P. O. Box 241 Elkton, MD 21921
3	Thiokol Corporation Wasatch Divison ATTN: S. J. Bennett P. O. Box 524 Brigham City, UT 84302

No. of Copies	Organization
1	United Technologies Research Center ATTN: A. C. Eckbreth East Hartford, CT 06108
3	United Technologies Corp. Chemical Systems Division ATTN: R. S. Brown T. D. Myers (2 copies) P. O. Box 49028 San Jose, CA 95161-9028
1	**Universal Propulsion Company** **ATTN: H. J. McSpadden** **25401 North Central Ave.** **Phoenix, AZ 85027-7837**
1	Veritay Technology, Inc. ATTN: E. B. Fisher 4845 Millersport Highway P. O. Box 305 East Amherst, NY 14051-0305
1	Brigham Young University Dept. of Chemical Engineering ATTN: M. W. Beckstead Provo, UT 84058
1	California Institute of Technology Jet Propulsion Laboratory ATTN: L. Strand/MS 512/102 4800 Oak Grove Drive Pasadena, CA 91109
1	California Institute of Technology ATTN: F. E. C. Culick/MC 301-46 204 Karman Lab. Pasadena, CA 91125
2	Purdue University School of Mechanical Engineering ATTN: N. M. Laurendeau S. N. B. Murthy TSPC Chaffee Hall West Lafayette, IN 47906
1	Rensselaer Polytechnic Institute Department of Chemical Engineering ATTN: A. Fontijn Troy, NY 12181
2	University of California, Santa Barbara Quantum Institute ATTN: K. Schofield M. Steinberg Santa Barbara, CA 93106

No. of Copies	Organization
1	University of Colorado at Boulder Engineering Center ATTN: J. Daily Campus Box 427 Boulder, CO 80309-0427
2	University of Southern California Department of Chemistry ATTN: S. Benson C. Wittig Los Angeles, CA 90007
1	Cornell University Department of Chemistry ATTN: T. A. Cool Baker Laboratory Ithaca, NY 14853
1	University of Delaware ATTN: T. Brill Department of Chemistry Newark, DE 19711
1	University of Florida Department of Chemistry ATTN: J. Winefordner Gainesville, FL 32611
3	Georgie Institute of Technology School of Aerospace Engineering ATTN: E. Price W. C. Strahle B. T. Zinn Atlanta, GA 30332
1	Johns Hopkins University /APL Chemical Propulsion Information Agency ATTN: T. W. Christian Johns Hopkins Road Laurel, MD 20707
1	University of Michigan Gas Dynamics Lab Aerospace Engineering Bldg. ATTN: G. M. Faeth Ann Arbor, MI 48109-2140

USER EVALUATION SHEET/CHANGE OF ADDRESS

This laboratory undertakes a continuing effort to improve the quality of the reports it publishes. Your comments/answers below will aid us in our efforts.

1. Does this report satisfy a need? (Comment on purpose, related project, or other area of interest for which the report will be used.) _____

2. How, specifically, is the report being used? (Information source, design data, procedure, source of ideas, etc.) _____

3. Has the information in this report led to any quantitative savings as far as man-hours or dollars saved, operating costs avoided, or efficiencies achieved, etc? If so, please elaborate. _____

4. General Comments. What do you think should be changed to improve future reports? (Indicate changes to organization, technical content, format, etc.) _____

BRL Report Number BRL-TR-3369 Division Symbol _____

Check here if desire to be removed from distribution list. ____

Check here for address change. ____

Current address: Organization _____
Address _____

DEPARTMENT OF THE ARMY
Director
U.S. Army Ballistic Research Laboratory
ATTN: SLCBR-DD-T
Aberdeen Proving Ground, MD 21005-5066

OFFICIAL BUSINESS

BUSINESS REPLY MAIL
FIRST CLASS PERMIT No 0001, APG, MD

Postage will be paid by addressee.

Director
U.S. Army Ballistic Research Laboratory
ATTN: SLCBR-DD-T
Aberdeen Proving Ground, MD 21005-5066

NO POSTAGE
NECESSARY
IF MAILED
IN THE
UNITED STATES